Hindawi
Advances in Meteorology
Volume 2018, Article ID 9341026, 16 pages
https://doi.org/10.1155/2018/9341026

Research Article

Studies on the Climate Effects of Black Carbon Aerosols in China and Their Sensitivity to Particle Size and Optical Parameters

Xingxing Ma, Hongnian Liu, Xueyuan Wang, and Zhen Peng

School of Atmospheric Sciences, Nanjing University, Nanjing 210023, China

Correspondence should be addressed to Hongnian Liu; liuhn@nju.edu.cn

Received 12 April 2018; Revised 4 September 2018; Accepted 9 October 2018; Published 21 November 2018

Academic Editor: Roberto Fraile

In this paper, based on the principle of Mie scattering, we calculated the optical parameters of BC aerosols at different scales and then applied the new optical parameters to simulate the BC aerosols concentration distribution, radiative forcing, and their climate effects. We also compared the results of optical parameters of BC aerosols with homogeneous scales and analyzed the effect on climate. Compared with the conventional uniform-scheme optical parameterization, the concentrations of the first mode of BC aerosols simulated with the optical parameters that were recalculated based on the particle size are significantly higher, while the concentrations of the other modes and the total of BC aerosols are lower. In the respective of statistics, the changes of column burdens of BC in four modes are 0.085, −0.095, −0.089, −0.054 mg/m^2. The clear-sky TRF of BC are weakened in the value of 0.03 W/m^2 averaged over the domain, while the all-sky TRF of BC are enhanced of 0.06 W/m^2 in general. The warming effect of BC becomes weaker when using the new scheme by −0.04 K to −0.24 K. When using the new optical parameters scheme, the regional average surface concentrations of BC in four modes are 0.372, 0.264, 0.055 and 0.004 μg/m^3, respectively. Especially, the first and the second mode account for as large as 53% and 38%. The surface concentration and column burden of total BC are 0.69 μg/m^3 and 0.28 mg/m^2 can be dropped. The regional average direct RFs of BC at the top of the atmosphere are 0.49 W/m^2 under clear-sky and 0.36 W/m^2 under all-sky averaged over the domain. Over most areas of central China, North China, and East China, BC may increase the temperature in a range of 0.05~0.15 K, while over South China, BC shows cooling effect. In average, the precipitation variations caused by BC over East China, North China, South China, and Northeast China are −0.83, −0.05, −0.11, and −0.13 mm/d, respectively. As a whole, the variations of circulation, pressure, and temperature show a good correspondence.

1. Introduction

Atmospheric aerosols can affect the earth's climate through both direct and indirect effects and play important roles in atmospheric radiation and climate change. Among all of the anthropogenic aerosols, black carbon (BC) aerosols can effectively absorb solar radiation in the visible and infrared bands to heat the atmosphere and affect the climate and air quality [1, 2] and therefore play a unique and important role in the climate systems. The Intergovernmental Panel on Climate Change (IPCC) report [3] indicates that the average direct radiative forcing of global BC aerosols is 0.4 W·m^{-2}. BC aerosols make an important contribution to global warming [4] and have become the second major warming factor after CO_2 [2].

East Asia is an important source region of global aerosol emissions [5]. The anthropogenic aerosols in East Asia have increased, which has had a nonnegligible influence on the regional climate. The global atmosphere model CAM3 was used to study the influence of sulfate aerosols and BC aerosols on the East Asian summer monsoon, and the results indicate that sulfate aerosols reduce the temperature in most areas of China, decreasing precipitation in some regions and weakening the East Asian summer monsoon [6]. BC aerosols also weaken the East Asian summer monsoon, but their influence is more complicated. The relationship between BC aerosols and regional precipitation has been studied, and researchers suggested that the BC aerosol emissions in China are related to the droughts in southern China and the floods in northern China over the past several decades [7]. BC

aerosols have a significant influence on the weakening of the wind velocity [8]. BC aerosols have a relatively heterogeneous spatiotemporal distribution, which makes it difficult to evaluate their influence on the regional climate. Coal combustion is the main anthropogenic source of BC aerosols [9]. Coal is the main component of the energy structure in China; therefore, several researchers have concluded that one quarter of the BC aerosols generated by global anthropogenic emissions comes from China [10, 11]. With the accelerated development in China in recent years, the emissions of BC aerosols have increased significantly, and BC aerosols in China have drawn broad international attention. China is located in the Asian monsoon area. The response of the climate in this region to the atmospheric compositions could be different from those in other regions, so it is necessary to use a regional model to study the radiative forcing and climate effect of BC aerosols in this region.

Aerosols affect atmospheric radiation through scattering and absorption, and their optical parameters are important for the calculation of radiation effects. In numerical simulations, the optical parameters of BC aerosols directly affect the calculated radiation effects. The radiative forcing effect of BC aerosols has received wide attention, and the analysis of their optical properties is especially important [12]. Many analyses of aerosol optical parameters have focused on dust and sulfates, and calculations of the optical properties BC aerosols are relatively limited. No analyses of the light extinction coefficient, absorption coefficient, and scattering phase function of BC aerosols have been conducted.

The climate forcing of carbon aerosols varies significantly with their size distribution [13, 14]. The average indirect radiative forcing effect of carbon aerosols at the top of the atmosphere ranges from −0.34 to 1.08 W/m^2, and its variation strongly depends on the assumed particle size distribution of the aerosols in the model [14]. The sensitive of BC aerosols climate effects on the particle size distribution is due to the two reasons: different assumptions of the particle size distribution will cause differences in the calculation of the BC aerosols' concentration distribution and then result in changes in the optical parameters of the BC aerosols. In many previous studies, the particle size distribution of BC aerosols adopted the homogeneous scale (median radius) method, and the optical parameters only varied with the wavelength. This method can cause relatively large errors and increase the uncertainty of the climate effects of BC aerosols.

Because the concentration of BC aerosols and the climate effect are relatively sensitive to the particle size, in previous studies, we adopted a size-resolved model of BC aerosols and studied the climate effect of BC aerosols based on the measured particle size distribution [15]. However, the optical parameters did not vary with the particle size, which may cause several errors. In this paper, we calculate the optical parameters of BC aerosols with different scales mainly through the principle of Mie scattering and further use the calculated optical parameterization scheme to simulate the size-resolved climate effects of BC aerosols. The conventional scale division scheme for the BC aerosols was used [15]. We compare the differences in the simulation results caused by the differences in the optical parameterizations of BC aerosols.

2. Calculation of the Optical Coefficient of Black Carbon Aerosols

In numerical models, the optical coefficient of aerosols directly affects the calculated radiation effect, and the radiation transfer scheme usually requires three input parameters: single scattering albedo (SSA), dissymmetry factor (DF), and mass absorption coefficient (MAC). The acquisition of these three optical parameters must be based on Mie scattering theory.

The SSA (ω_0) is the ratio between the aerosol scattering coefficient and the light extinction coefficient, and it measures the absorption strength of aerosols. It is an important optical property of aerosols. The MAC (K) measures the absorption properties of a unit aerosol mass, and the DF (g) describes the asymmetry of the forward and backward scatterings of aerosols. In numerical models, these parameters play important roles in calculating the radiative forcing of aerosols.

The three conditions for the numerical calculation are (1) the complex refractive index of BC aerosols in different wave bands, (2) the spectral distribution of the BC aerosols, and (3) the program of Mie scattering theory.

2.1. Complex Refractive Index. The real and imaginary parts of the complex refractive index of aerosol particles represent the characteristics of scattering and absorption, respectively, and the magnitudes of the absolute values determine the strengths of the scattering and absorption properties of aerosols, which have a direct influence on the radiation of aerosols. For a given scale spectrum of particles, the variation in the radiation characteristics of aerosols with the wavelength is determined by its complex refractive index. Figure 1 shows the values of complex refractive index of BC aerosols. These values of the complex refractive index used by Shettie are selected in this paper [16]. This data source has also been used to study the optical properties of BC aerosols by others [17]. The variation of the imaginary part of the complex refractive index of BC aerosols with the wavelength is relatively small, but its absolute value is usually greater than 0.4; therefore, BC aerosols mainly absorb the long radiation.

2.2. Particle Size Distribution. The particle size of the aerosols also has an important effect on the final radiation. In previous studies, the RIEMS2.0 model divided BC aerosols into four bins, which somewhat improves the simulation performance of the model. We use the same division and assign different optical parameters to BC aerosols of every particle size bin according to the Mie scattering theory.

Using the program of the Mie scattering model, we calculate the SSA, DF, and MAC of the BC aerosols in different bands.

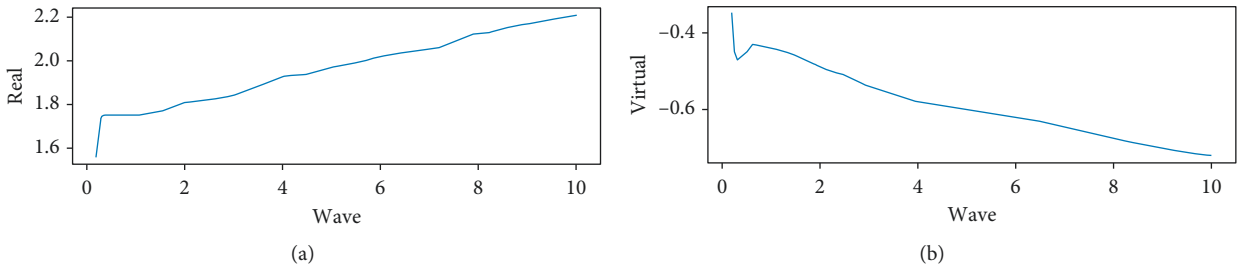

Figure 1: Complex refractive index of BC aerosols in different wavelengths.

Because the radiation parameters of BC aerosols have an important relationship with the particle size distribution, the spectral distribution of the particles is very important to numerical calculations of the optical parameters. Winchester et al. [18] indicated that a lognormal distribution can accurately describe the spectral distribution of particles. Other study also adopted a lognormal distribution to describe the spectral distribution of aerosols [19]. In this chapter, we adopt this distribution for the calculations:

$$\frac{dN(r)}{d\ln r} = \frac{N_0}{\sigma\sqrt{2\pi}} \exp\left(-\frac{\ln\left(r/r_g\right)^2}{2\sigma^2}\right). \quad (1)$$

Based on the division of BC aerosol particle sizes, we consider BC with four bins (i.e., BC1, BC2, BC3, and BC4) with radii of 0.075, 0.205, 0.48, and 2.7 μm, respectively. In Equation (1), the values of r_g and N_0 are from the results of Levy et al. [4]. Based on the conversion between the median radius and the distribution radius of the number concentrations, we obtain the radius distribution of the number concentrations for four modes, r_g:

$$r_g = r_v \exp\left(-3\sigma^2\right). \quad (2)$$

In Equation (1), N_0 represents the particle number density of BC aerosols, and we can calculate different values of N_0 from r_g under the different modes. V_0 is the amplitude of the volume distribution. σ represents the standard deviation of the radius:

$$N_0 = V_0 \frac{3}{4\pi r_g^3} \exp\left(-\frac{9}{2}\sigma^2\right),$$
$$V_0 = \int_0^\infty \frac{dV}{d\ln r} d\ln r. \quad (3)$$

2.3. Mie Scattering Model. In using the Mie scattering theory to calculate the solution, we assume that the particles are spheres, and we can obtain the relevant optical characteristics (optical coefficient) based on the radius and complex refractive index of the particles. The Mie scattering is based on the Maxwell equation, and it assumes that the vector wave equation has separable solutions and is derived in the spherical coordinate system. Many studies have focused on numerical algorithms for Mie scattering, and the complete process is described by Liou, who used the Legendre function and Bessel function [20].

Figure 2 shows the numerical calculation results of the optical coefficients of BC in four particle sizes bins. BC1, BC2, BC3, and BC4 represent BC particles with a radius of 0.075, 0.205, 0.48 and 2.7 μm, respectively. BC5 represents the BC optical parameters in the conventional scheme.

As shown in the figure, BC aerosols in different modes show different absorption ability. BC5 in the conventional scheme shows the highest absorption while BC1, BC2, BC3, and BC4 show lower absorption in order.

The optical parameters of the BC aerosols used in the conventional model are taken from database of the University Corporation for Atmospheric Research (UCAR) (http://www.ccsm.ucar.edu/models/atm-cam/download/) and are not differentiated based on the particle size. BC5 represents the conventional settings of the optical parameters. A comparison of the results shows that the calculated optical parameters for the first mode of BC aerosols (particle size of 0.075 μm) are most similar to those of the conventional settings, and the calculated MAC is smaller than that of the conventional settings.

3. Design of the Numerical Scheme

In this paper, we use the RIEMS2.0 model, and the emission source data are taken from the MEIC-2010 emissions inventory, which has a spatial resolution of 0.25° × 0.25°. The time period of the numerical experiments is from January 1, 2010 to December 31, 2010.

We input the optical coefficients of the BC aerosols calculated for the four particle sizes bins into the RIEMS2.0 model and simulate the concentration, direct radiation, and the climate effect of the BC aerosols. In addition, we compare and analyze the results with those obtained by the conventional simulation scheme of BC aerosols with uniform-scale-optical parameters (hereinafter referred to as Scheme 1) [15]. In the following analysis, the scheme used in this paper is called the size-resolved scheme of optical parameters (referred to as Scheme 2), and the results show the differences between Schemes 2 and 1 simulation results. In this paper, we consider the direct radiative forcing effect of BC aerosols and its climate effect and compare them with the previously calculated direct radiative forcing and climate effects. The method used for the regional division is the same as those in Reference [15].

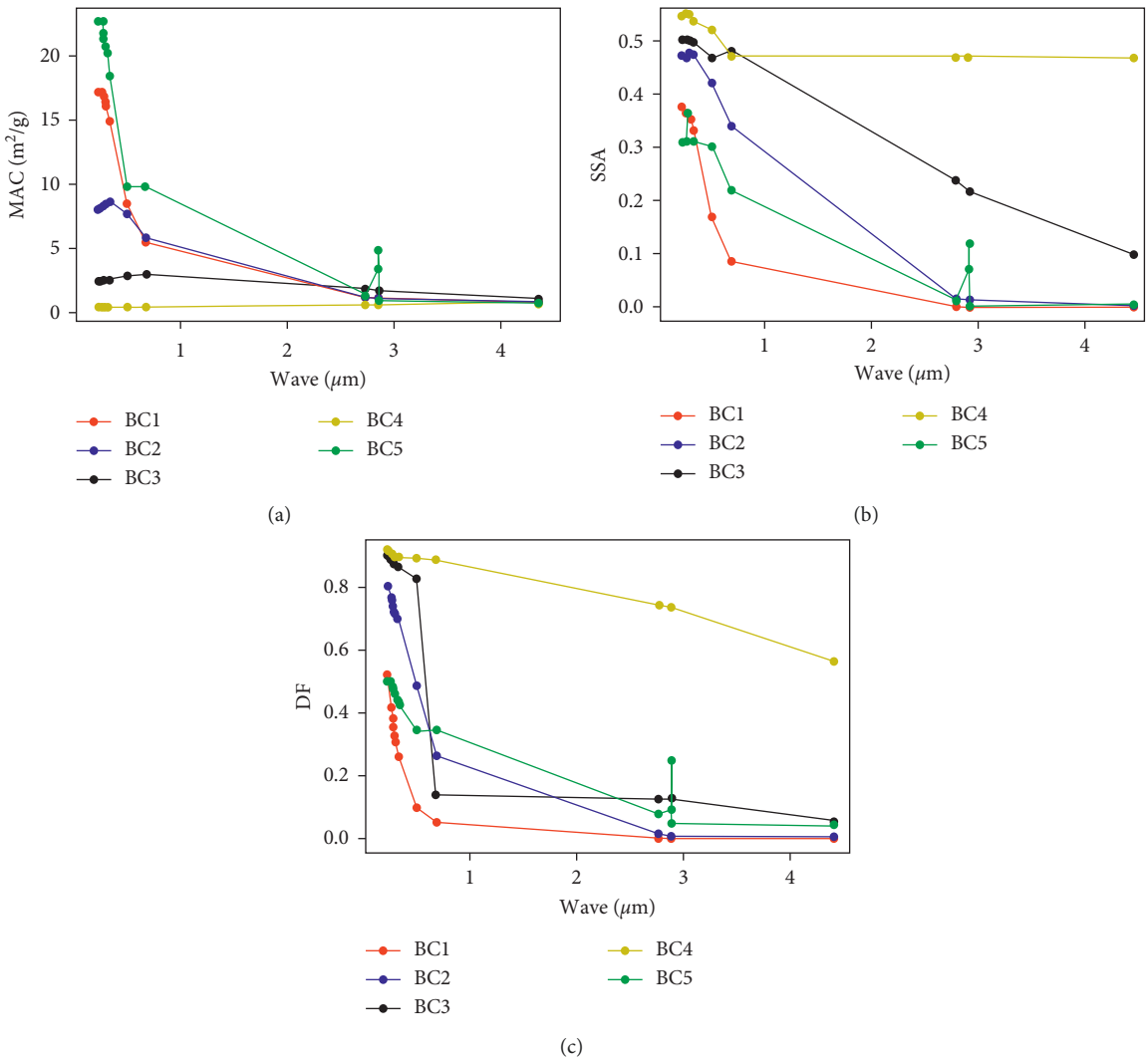

Figure 2: Variations of the optical properties of BC aerosols of different bins with the wavelength.

4. Results and Analysis

4.1. Difference between the Two Schemes of Optical Parameters on the Simulation of BC Aerosols. We use Schemes 1 and 2 to simulate the BC aerosols in China and find that there are differences in the concentrations, optical thicknesses, direct radiative forcing, and climate effects of the BC aerosols simulated using the two optical parameterization schemes.

The differences between the ground surface concentrations of BC aerosols simulated by the two schemes of optical parameters (Figure 3) show that the BC aerosol concentration of the first mode simulated by Scheme 2 is significantly higher, and the maximum difference is 3.30 $\mu g/m^3$. The ground surface concentrations of the other modes of BC aerosols are lower under Scheme 2. The total ground surface concentrations of BC aerosols are also lower under Scheme 2, and the range of differences is −0.2 to −2.8 $\mu g/m^3$. The differences in the regional average concentrations of the four modes of BC aerosols and in the total BC aerosol ground surface concentrations are 0.24, −0.16, −0.18, −0.10, and −0.21 $\mu g/m^3$, respectively.

The average variations in the column concentrations of the different modes of BC aerosols are 0.085, −0.095, −0.089, and −0.054 mg/m^2, respectively, and the total column concentrations of BC aerosols decrease by 0.08–0.56 mg/m^2. The distributions of the variations in the column concentrations of BC aerosols are similar to that of the ground surface concentrations (not shown). The differences in the BC aerosol concentrations occur due to the different optical parameters, which has the complicated feedback effect in the aerosol-radiation-meteorological field could generate different meteorological fields, and further affect the transport and diffusion of aerosols.

The optical thicknesses simulated by Scheme 2 are lower than those simulated by Scheme 1 and the differences range from −0.008 to −0.0064 (figure omitted). In the region of high BC aerosol optical thicknesses, the differences between the simulations are relatively large. For example, in the region near the Sichuan Basin and the North China Plain, the difference is approximately −0.0064; in the area with lower optical thicknesses, the differences are smaller. The regional

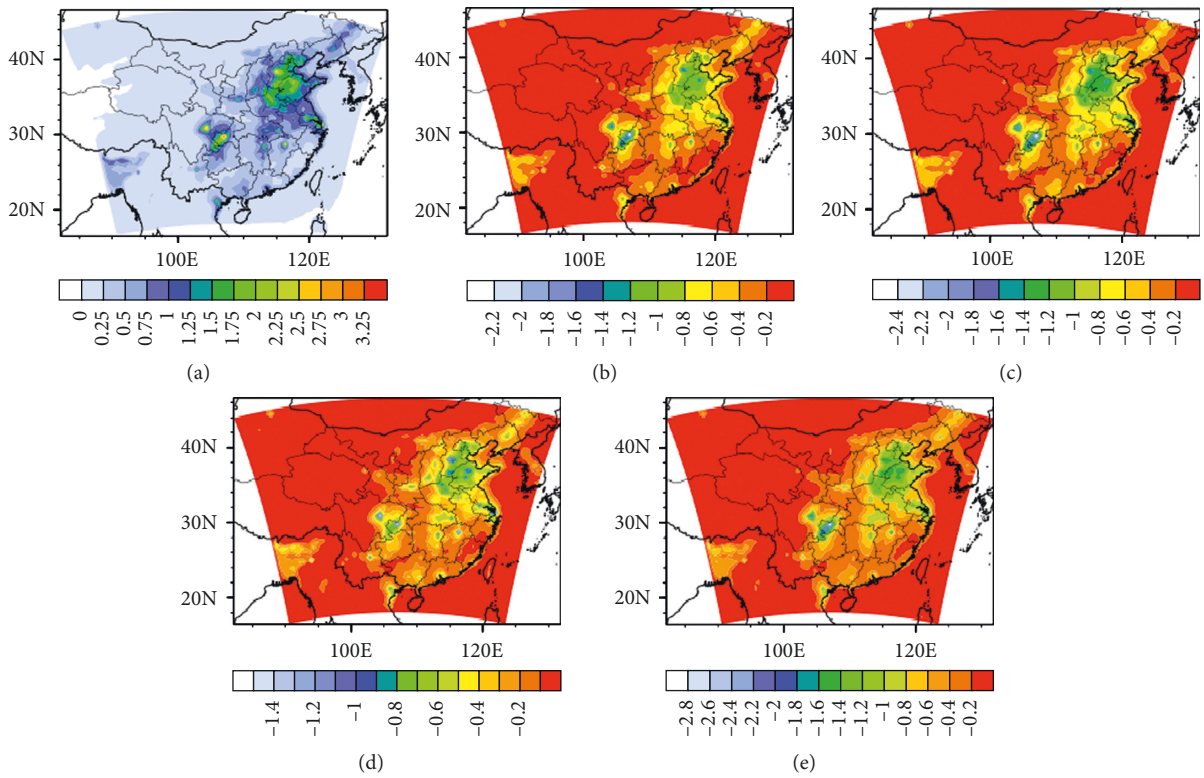

FIGURE 3: Differences between the four modes and the total ground surface concentrations of BC aerosols calculated by the two schemes ($\mu g/m^3$). (a) BC1. (b) BC2. (c) BC3. (d) BC4. (e) BC (total).

average difference in the BC aerosol optical depth (AOD) is −0.0019. The causes of the differences in optical thickness include the differences in the concentrations and the differences in the optical parameters.

Figure 4 shows the distributions of the differences in climate effects of BC aerosols simulated with two optical parameterization schemes. The direct radiative forcings under all-sky conditions simulated by Scheme 2 are higher than those from Scheme 1 with the range of 0.1–0.7 W/m^2 in most regions of central and eastern China but are slightly lower near the Sichuan Basin. The differences in clear-sky top-of-atmosphere radiative forcing (TRF) are negative in most areas. In the North China Plain and South China, the TRF changes by −0.2 to −0.8 W/m^2; near the Sichuan Basin, there is a region of strongly negative variations of TRF with a maximum value of −0.94 W/m^2, which is consistent with the variations in the BC aerosol optical depth. Over south of the Sichuan Basin, the clear-sky TRF of BC is also intensified, but the range of enhancement is smaller than that of the all-sky TRF, which is approximately 0.2–0.4 W/m^2. The regional average clear-sky TRF of BC aerosols is 0.034 W/m^2 lower, whereas the all-sky TRF is 0.06 W/m^2 higher. In general, in comparison with the change of the all-sky TRF, the variation in the clear-sky direct TRF of BC aerosols is more similar to the distributions of the variations in the concentration. Using the size-resolved optical parameters, the total concentration of BC aerosols, the simulated AOD, and TRF are lower. Because the calculation of the all-sky TRF considers the complicated influence of clouds, there are several differences between the changes in the all-sky TRF of BC aerosols and the changes in the other variables. Some research results also show that the effects of BC on clouds vary between regions and present much uncertainty [21].

The use of the principle of Mie scattering to calculate the size-resolved optical parameters causes a change in the direct climate effect of BC aerosols. The ground surface temperatures simulated by the two schemes increase in many regions, and there are several similarities. However, the extents of the warming regions simulated by Scheme 2 are smaller, and the magnitudes of the warming are lower in some regions, which is consistent with the weakening of the clear-sky TRF of BC in these regions. In Northeast China, the warming effect of BC is enhanced by 0.04 to 0.16 K. Figure 4(b) shows that this region also has significant increase in the clear-sky TRF of BC aerosols. In addition, in the Beijing-Tianjin-Hebei area and the Shandong Peninsula, the warming effect of BC is intensified by 0 to 0.16 K. BC simulated by the two schemes mostly have cooling effects in the arid and semiarid areas of western China. The cooling effects simulated using Scheme 2 are greater in some regions, and the cooling ranges from −0.04 to −0.24 K. The simulation of BC using Scheme 2 results in increased precipitation in South China, and the variations range from 0.4 to 2.4 mm/d. In some regions in the middle and lower reaches of the Yangtze River Basin, BC aerosols cause greater reductions in

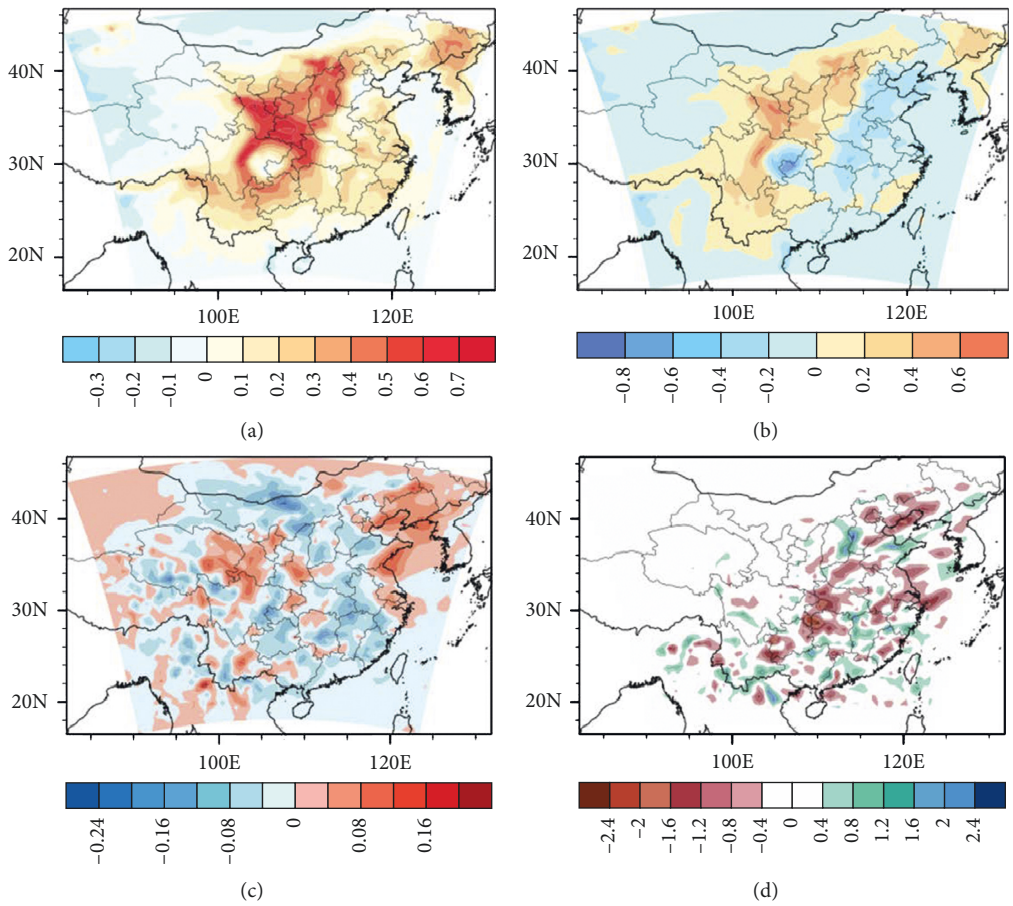

Figure 4: Differences between the climate effects of BC aerosols simulated by the two parameterization schemes. (a) All-sky top-of-atmosphere radiative forcing (TRF; W/m^2). (b) Clear-sky TRF (W/m^2). (c) Temperature (K). (d) Precipitation (mm/d).

precipitation, and the variations of precipitation range from −0.4 to −2.4 mm/d. In Northeast China and some regions in North China, BC aerosols simulated by Scheme 2 reduce the precipitation, whereas the results of Scheme 1 are the opposite. The climate effects of aerosols show much uncertainty due to many factors and so far the mechanism has not been formed [22]. Compared to the effects on temperature, the effects of BC on precipitation are more unclear by the research [23]. In general, BC aerosols show a complicated influence on precipitation, and the sensitivity of optical parameterization schemes makes it more difficult to analyze, which merits further studies.

4.2. The Climate Effect of BC Aerosols with the Size-Resolved Scheme of Optical Parameters. The results described above indicate that the radiative forcing and climate effect of BC aerosols are relatively sensitive to the optical parameters. If the dependence of the BC aerosols' optical parameters on the particle size is not considered in simulations of the climate effect of BC aerosols, errors may occur. In this section, we analyze the distribution of BC aerosol concentrations and its climate effect for the distribution scheme that considers the dependence of the aerosols' optical parameters on the particle size (Scheme 2).

4.2.1. Concentration Distribution of BC Aerosols. Figure 5 shows the spatial distributions of the annual average ground surface concentrations for the four modes and the total of BC aerosols simulated using Scheme 2. Figures 5(a)–5(d) show the results for the modes of BC aerosols with sizes of 0.075, 0.205, 0.48, and 2.7 μm, respectively, and Figure 5(e) shows the results for the total BC aerosols. The spatial distributions of BC aerosols with different particle sizes are similar, and the ground surface concentrations decrease from east to west, which is generally consistent with the emissions distribution of BC aerosols. In the North China Plain, Yangtze River Delta, and Sichuan Basin, which have dense industries and relatively high population densities, the BC aerosol concentrations are relatively high. Although the BC aerosol distributions of the four modes are similar, there are differences between the modes. The regional average ground surface concentrations of the four modes of BC aerosols are 0.372, 0.265, 0.055, and 0.004 μg/m^3, respectively. Before we adjust the optical properties of BC aerosols based on the particle size, the simulated proportions of the four modes are essentially consistent with their initial emissions proportions, whereas after recalculating the optical parameters according to Mie

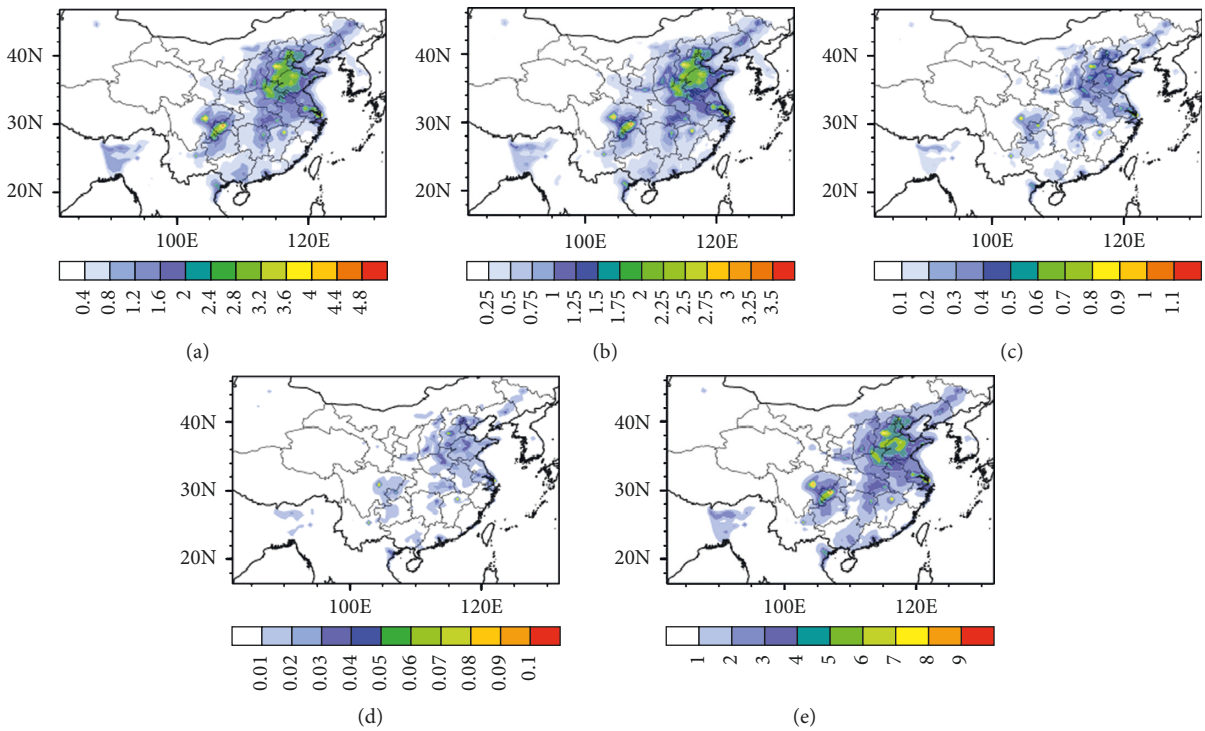

Figure 5: Distributions of the different modes and the total ground surface concentrations of BC aerosols ($\mu g/m^3$). (a) BC1. (b) BC2. (c) BC3. (d) BC4. (e) BC (total).

scattering, there are obvious differences in the proportions of the four modes. The proportions of the first and second modes, which have relatively small aerosol radii, are 53% and 38%, respectively, and the proportions of the third and fourth modes are very small, especially the fourth mode. The range of the total ground surface concentrations of BC aerosols in North China and East China is 1–6 $\mu g/m^3$ (Figure 5(e)). In the lower reaches of the Yellow River and the Yangtze River Basin, as well as the Sichuan Basin, there are regions of high BC aerosol ground surface concentrations, and the maximum concentration reaches 9.83 $\mu g/m^3$. The regional average total ground surface concentration of BC aerosols is 0.70 $\mu g/m^3$. The distribution of column concentrations of BC aerosols is similar to the distribution of ground surface concentrations (not shown). The regional average column concentration of the first mode of BC aerosols is the highest (0.15 mg/m^2) and that of the second mode is slightly lower (0.10 mg/m^2). The regional average total BC aerosol column concentration is 0.28 mg/m^2, and the maximum is 2.05 mg/m^2. In most other regions except for the arid and semiarid areas in western China, the range of BC aerosol column concentration is 0.20–2.0 mg/m^2.

The distributions of BC aerosol ground surface concentrations in this study are similar to the results of previous studies, but the concentrations in this study are smaller, which could be caused by the size-resolved scheme [24, 25]. Because many previous studies adopted a particle size distribution scheme with a constant scale and simply assumed the radius of BC aerosols to be approximately 0.1 μm [26–28]. They did not accurately consider the presence of BC aerosols with larger particle sizes, which caused the simulated BC aerosol concentrations to be higher than they actually are.

The wind field at the 850 hPa height during the spring (figure omitted) shows that the eastern part of the Indian Peninsula is mainly affected by westerly airflow, and the BC aerosols accumulate. In China, regions of high concentrations of BC aerosols are located in the Sichuan Basin and North China Plain. There are many mountains and hills in the Sichuan Basin, and the topography makes it difficult for pollutants to diffuse. The westerly airflow also causes the accumulation of BC aerosols in this region, which causes the concentration of BC aerosols to be very high. The high-concentration region in the North China Plain is mainly caused by industrial and anthropogenic emissions. In the summer, southern China and the Indian Peninsula are both affected by southwesterly airflows, and long narrow areas of high BC aerosol concentrations form in the Sichuan Basin and eastern China. Compared with the spring, the climate characteristics of northward and eastward transportation are obvious in southern China, and the column concentrations of BC aerosols increase in eastern China. Northwesterly airflows prevail in most regions north of the Yangtze River; therefore, the high-concentration area of BC aerosols in the North China Plain weakens. In the fall, the distribution of column BC aerosol concentrations is similar to those in the other seasons, but the concentrations are lower; southerly winds prevail in most of central and eastern China. In the winter, northwesterly winds prevail to the north of the Yangtze River,

and easterly winds prevail to the south of the Yangtze River. The concentrations of BC aerosols in North China are higher than that in the fall.

To validate the effect of models on the simulation of BC aerosol concentrations, we compare the simulated BC aerosol concentrations with observations. The observed values in different regions are obtained from several studies [29–36]. The simulated and observed annual average concentrations of BC aerosols in different regions of China and the linear relationship between the data have been studied (figure omitted). The straight black line is the fit between the observed values and simulated values, and the different symbols represent different regions.

The results show that the model can simulate the ground surface concentrations of BC aerosols relatively well, and the correlation coefficient with the observations is 0.78. The linear relationship is given by the equation $y = 0.78x + 0.29$. In general, the simulated values are lower than the observed values, which is likely because the emission source we used does not consider straw combustion. The simulated BC aerosol concentrations of Zhuang et al. [37] are also lower than the observed values.

Figure 6 compares the monthly variations in the simulated BC aerosol ground surface concentrations with the observed values. The black dotted lines represent the simulated BC aerosol ground surface concentrations, the red dots represent the observations, and the red vertical line segments represent the standard deviations. The observation data are from the Atmospheric Composition Observation Network of the China Meteorological Administration and mainly include the observed concentrations of BC aerosols averaged over two years (2006 and 2007) at fourteen stations. In the areas of Longfengshan, Jinsha, Taiyangshan, Nanning, and Chengdu, the simulation results and observations are relatively consistent. In the winter, in Jinsha and Zhengzhou stations, the model-simulated BC aerosol concentrations are lower than the observations. At most stations, the observations are low in the summer and high in the winter. Except for the stations in Gucheng, Dalian, and Gaolanshan, the model simulates the monthly variations in the BC aerosol concentrations relatively well. In Xi'an, Dunhuang, and Lhasa, the simulated concentrations of BC aerosols are significantly lower than the observations, which is likely because the anthropogenic emission sources in western areas are difficult to estimate. This problem was also found in a similar study [25].

4.2.2. Optical Thickness Distribution and Radiative Forcing of BC Aerosols. Similar to the distribution of column concentrations, the regions of high BC aerosol optical thicknesses are located in North China and the Sichuan Basin (figure omitted). In most areas of North China and East China, the BC aerosol optical thicknesses range from 0.003 to 0.006. In the Sichuan Basin, the middle and lower reaches of the Yellow River and the Yangtze River Basin, and the Yangtze River Delta, the optical thicknesses of the BC aerosols are greater. In these regions, the industry is more well-developed, economic development has occurred more rapidly, and the population density is higher, which leading to higher emissions and therefore inducing greater BC aerosol concentrations. The regional average BC aerosol optical thickness is 0.0013, and the maximum is 0.0073. The model can simulate the spatial distribution of the BC aerosol optical thicknesses relatively well, and the distribution is similar to the results of previous studies [38, 39]. However, the simulated optical thicknesses of BC aerosols in this study are slightly lower than those in some early studies [40].

Figure 7 shows the distributions of the all-sky TRF and clear-sky TRF of BC aerosols. The distributions of the TRF are similar to the distributions of the BC aerosol emissions and concentrations. However, the radiative forcing is affected by the aerosol mass as well as by the vertical structure of the aerosols, optical properties, ground surface albedo, and clouds [41]. Therefore, there is a difference between the distribution of the BC aerosol radiative forcing and the concentrations. The all-sky TRFs of BC aerosols have a range of 0–2.0 W/m^2. The high values are located near the Sichuan Basin and in Northeast China, and the maximum TRF is 2.11 W/m^2. In the region between the Yangtze River and the Yellow River Basin, the all-sky TRFs of BC aerosols are relatively strong (1.4–1.8 W/m^2). The TRFs of BC aerosols under the clear-sky conditions are lower (0–1.8 W/m^2); the high values are located north of the Yellow River, and the maximum value is 1.98 W/m^2, which is similar to the distribution of the BC aerosol optical thicknesses. In comparison with the all-sky TRFs, the distribution of the clear-sky TRFs is more similar to the distribution of the optical thicknesses. This is because the all-sky TRF is also affected by the mass and cloud water content of the aerosols, so it is more complicated. The regional average clear-sky and all-sky TRFs of BC aerosols are 0.49 and 0.36 W/m^2, respectively, which are similar to the global average BC aerosol TRF (0.4 W/m^2) in the IPCC report [3]. In the same class of research areas, the regional average of the BC aerosol direct TRF estimated by Chang and Park [42] is 0.5 W/m^2, and the BC aerosol TRFs calculated by Wu et al. [43] range from 0.5 to 4.1 W/m^2. The regional average TRF of BC aerosols estimated by Li et al. [25] is 1.22 W/m^2, and the maximum is 5-6 W/m^2, whereas the average and maximum BC aerosol TRFs simulated by Zhuang et al. in 2010 [37] are 0.75 and 5.5 W/m^2, respectively. In Chang et al. [44], the regional average TRF of BC aerosols is 0.58 W/m^2. The results of this study are lower than those in these previous studies. This is because the size-resolved scheme assumes that a proportion of the BC aerosols is larger and has weaker optical properties. In the numerical model, the radiation effect of BC aerosols is weakened by a feedback effect between the concentration and other physical quantities. If we do not consider the particle size distribution of BC aerosols and their optical parameters, the climate effect of BC aerosols will likely be overestimated.

4.2.4. Influence on Temperature and Precipitation. BC aerosols change the energy equilibrium in the atmosphere through the absorption of solar radiation and cause changes in the dynamic-thermodynamic circulation. Figure 8 shows the effects of BC aerosols on the annual

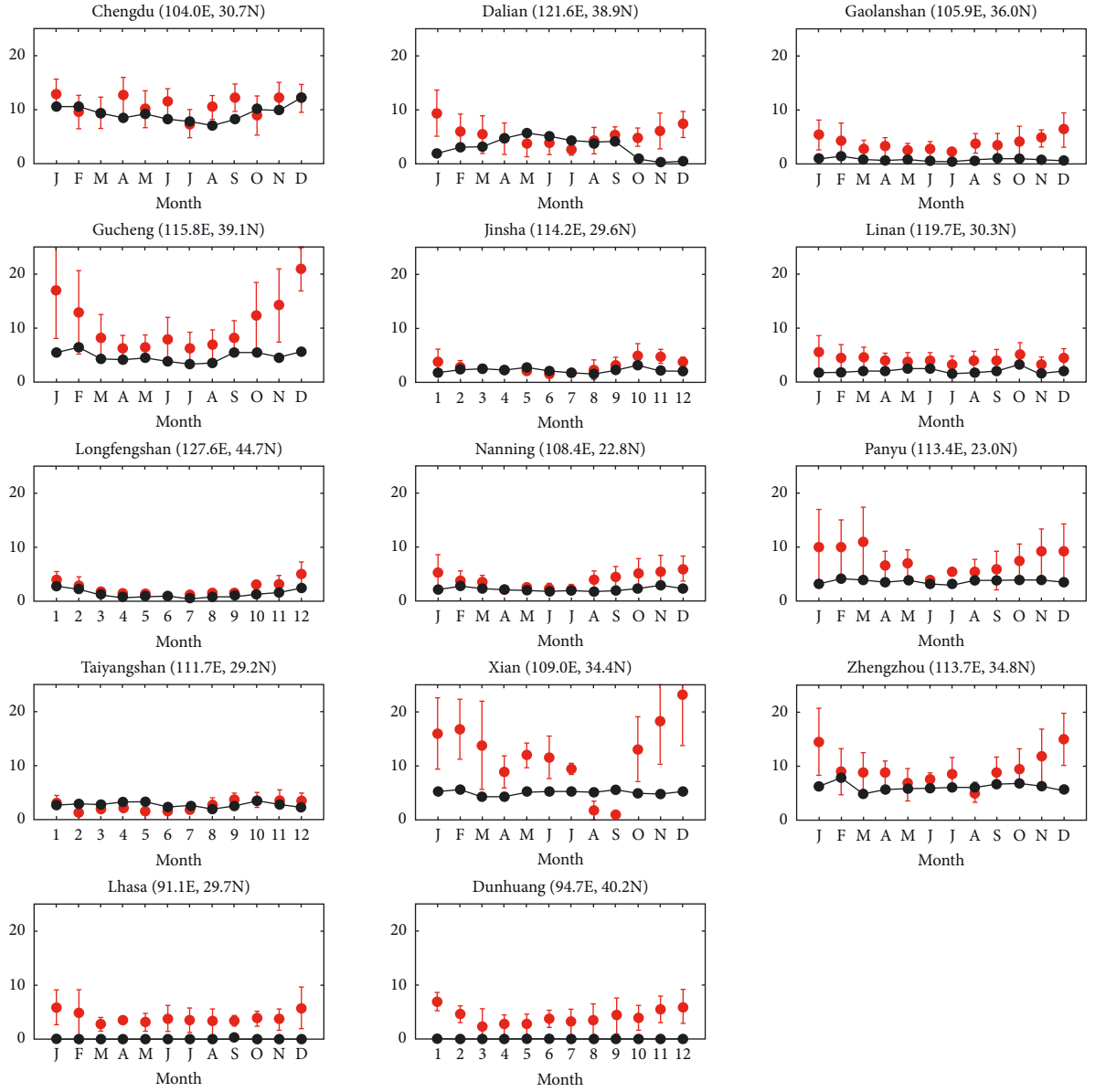

Figure 6: Comparison of the observed and simulated monthly changes in the BC aerosol concentrations ($\mu g/m^3$) in different regions of China. The black dotted lines represent the simulated BC aerosol ground surface concentrations, the red dots represent the observations, and the red vertical line segments represent the standard deviations.

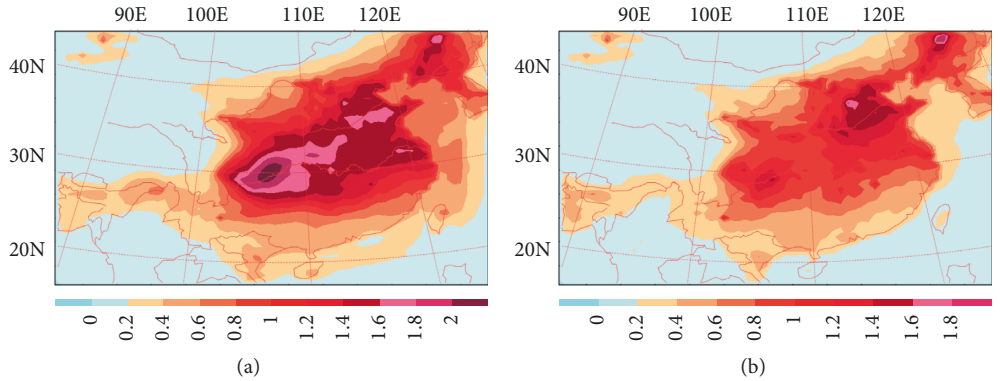

Figure 7: Top-of-atmosphere radiative forcing (TRF; W/m^2). (a) All-sky TRF. (b) Clear-sky TRF.

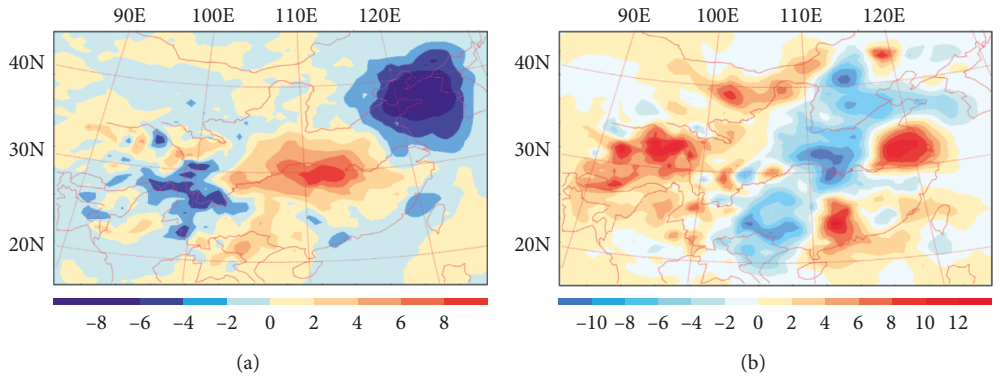

Figure 8: Sea surface pressure (Pa) changes caused by BC aerosols. (a) Summer. (b) Winter.

average ground surface temperature and annual average precipitation. In most regions of East China, North China, and central China, the BC aerosols cause increases in the ground surface temperature, and the changes range from 0.05 to 0.15 K. In particular, the warming is significant in some regions between the Yangtze River and Yellow River Basin and near the Sichuan Basin, and the maximum warming is 0.17 K. These regions also have high values of the BC aerosol radiative forcing. Therefore, there is the relatively good relationship between the influence of BC aerosols on the ground surface temperature and their radiative forcing. In parts of South China and Northwest China, BC aerosols cause cooling, varying from 0.05 to 0.15 K. At a regional scale, BC aerosols cause ground surface warming in North China, East China, and central China with average temperature changes of 0.034 K, 0.037 K, and 0.020 K, respectively, and has a cooling effect in South China. Because the emissions of BC aerosols are concentrated in central and eastern China, the radiative forcing of BC aerosols in the western area is relatively weak. However, Figure 9(a) shows that BC aerosols cause changes in the ground surface temperature in many regions of western China. This is because the large-scale transfer process of BC aerosols can change the properties of clouds in relatively distant regions and thus affect the climate, and it can also change the climate at short distances through its influences on the circulation, water vapor transportation, and cloud distribution [45]. It is worth noting that the distribution of strong BC aerosol radiative forcing is roughly consistent with the high value region of ground surface warming caused by BC aerosols. However, there are also several regions in which strong BC aerosol radiation causes decreases in the ground surface temperature. This phenomenon is possibly due to the influences of complicated regional cloud systems and precipitation, which also reflect the complicated BC aerosol-cloud feedback mechanism [40]. In several previous studies, the ranges of temperature changes caused by BC aerosols in East China and the eastern region of East Asia are −0.6 to 0.3 K and −0.4 to 0.1 K, respectively, which are greater than the climate effects of BC aerosols simulated in this study [46, 47]. Considering the particle size distribution of the optical parameters of BC aerosols causes the climate effect of BC aerosols to weaken.

The change in precipitation caused by BC aerosols is more complicated and has a greater regional uncertainty (Figure 9(b)). In parts to the south of the Yangtze River, the southeast coastal area, and north of the Yellow River, the BC aerosols increase the precipitation, varying from 0.5 to 2.5 mm/d. However, in some regions to the north of the Yangtze River and central China, the BC aerosols cause decreases in precipitation, and the range of the decreases is 0.5–3.0 mm/d. At a regional scale (Table 1), the BC aerosols cause decreases in precipitation in central China, North China, South China, and Northeast China, and the variations are −0.83, −0.05, −0.11, and 0.13 mm/d, respectively. In central China, the BC aerosols cause the precipitation to increase by 0.01 mm/d; for the entire simulation domain, the average decrease in precipitation caused by BC aerosols is 0.02 mm/d. BC aerosol emissions and precipitation in China are correlated over the past several years [7]. BC aerosols can cause increases in precipitation in southern China and decreases in precipitation in northern China. This study found that the precipitation in the northern regions decreases. However, the regional average precipitation in the southern regions decreases, which is likely associated with the differences between the models and different regional divisions. Due to the complexity of the influences of BC aerosols and precipitation in the climate system, there is still significant uncertainty in the relationship between BC aerosols and precipitation. Many studies have analyzed the influence of BC aerosols on precipitation in China. Several studies have indicated that BC aerosols cause decreases in precipitation in eastern China with a regional average reduction in precipitation of 0.09 mm/d [48], whereas other studies have indicated that BC aerosols can increase the precipitation and that the precipitation increased by 0.07 mm/d from 1950 to 2000 [44].

The influences of BC aerosols on the temperatures at different heights have been researched (figure omitted). At the 500 hPa height, BC aerosols cause warming in most regions of China. The range of warming is 0.01 to 0.05 K, which is significant in the region near the middle and lower reaches of the Yangtze River. On the other hand, in parts of Northeast China, BC aerosols cause cooling. The simulation at the height of 850 hPa indicates that BC aerosols

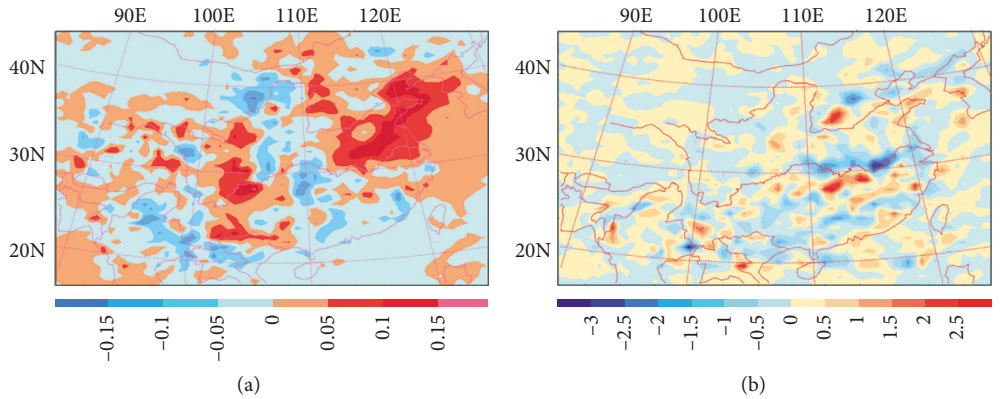

Figure 9: Annual average climate effects of BC aerosols. (a) Temperature (K). (b) Precipitation (mm/d).

Table 1: Regional average direct radiative forcing of BC aerosols and the climate effects.

	All-sky radiation at the top of atmosphere (W/m^2)	Clear-sky radiation at the top of atmosphere (W/m^2)	Temperature (K)	Precipitation (mm/d)
South China	0.70 (1.57)	0.47 (1.16)	−0.017 (−0.15)	−0.11 (−2.02)
Northeast China	0.90 (1.82)	0.79 (1.98)	0.002 (0.05)	−0.13 (−1.04)
North China	1.06 (1.73)	0.94 (1.85)	0.034 (0.12)	−0.05 (−2.19)
East China	1.36 (1.75)	0.94 (1.54)	0.037 (0.14)	−0.83 (−2.99)
Central China	1.01 (2.11)	0.75 (1.53)	0.020 (0.17)	0.01 (2.54)

Note: the values in the parentheses are the extreme values of the physical quantities.

cause increased temperatures near the Sichuan Basin and in the North China Plain as well as decreases in some regions of western China. A comparison of the influences of BC aerosols on the temperatures at these two heights shows that in the north of the Yellow River and near the Sichuan Basin, the warming caused by BC aerosols in the lower troposphere is more significant than that in the middle and upper troposphere. Therefore, the atmospheric instability in these regions increases, which may cause convective precipitation. Figure 8(b) shows that the precipitation in these regions also increases. A comparison of Figures 10(a) and 8(a) shows that at the 850 hPa height and at the ground surface, the distributions of the variations in the annual average temperatures caused by BC aerosols are similar.

4.2.5. Influences on the Circulation, Pressure, Temperature, and Precipitation in the Winter and Summer. The absorption of solar radiation by BC aerosols causes heating of the middle and lower atmosphere, and the airflow rises. The research indicates that BC aerosols can affect the wind changes in China [49]. Figure 11 shows the variations of the 850 hPa heights and the wind fields during the summer and winter. At the 850 hPa height, the decrease (increase) of the 850 hPa height field during the winter and summer caused by BC aerosols corresponds to a convergence (divergence) of the wind field. In the summer, the eastern region (near 110°E, 40°N) and central region (near 110°E, 30°N) of China correspond to low values and high values of height change, respectively. This region is located near the region of high BC aerosol emissions. In the winter, there are two dispersed regions of large height changes in central and eastern China. Correspondingly, BC aerosols cause the enhancement of the southwesterly airflow in the mid-latitude region during the summer and the intensification of the southerly airflow in the high-latitude region. The change of the wind field is the opposite during the winter, and the strength in the winter is stronger than that in the summer; it causes a clear divergence of the airflow in the region north of the Yangtze River and enhances the northerly wind during the winter. These changes in wind and height field caused by BC are similar to the results of other studies [37, 49].

Figures 12 and 8 show the influences of BC aerosols on the ground surface temperature and pressure field during the summer and winter. BC aerosols may cause the temperature increase or decrease between different areas [40]. Seen in the figure, in summer, except for some regions north of the Yellow River and a few areas along the eastern coast, the BC aerosols generally cause the ground surface temperature to decrease; at the 500 hPa height, however, the temperatures in most regions increase. It is assumed that the cooling effect caused by BC aerosols in South China and East China during the summer is induced by the complicated feedback and changes in the amount of clouds in the model, which merits further study [2, 50–52]. The region where the ground surface temperature decreases corresponds to an increase of the sea surface pressure. In most regions of South China and East China, the BC aerosols cause increases in the sea surface pressure, and the area of maximum pressure increase is located near the Sichuan Basin. This is because the cooling of the land over a large area causes the accumulation of the air mass, which results in increasing sea surface pressures

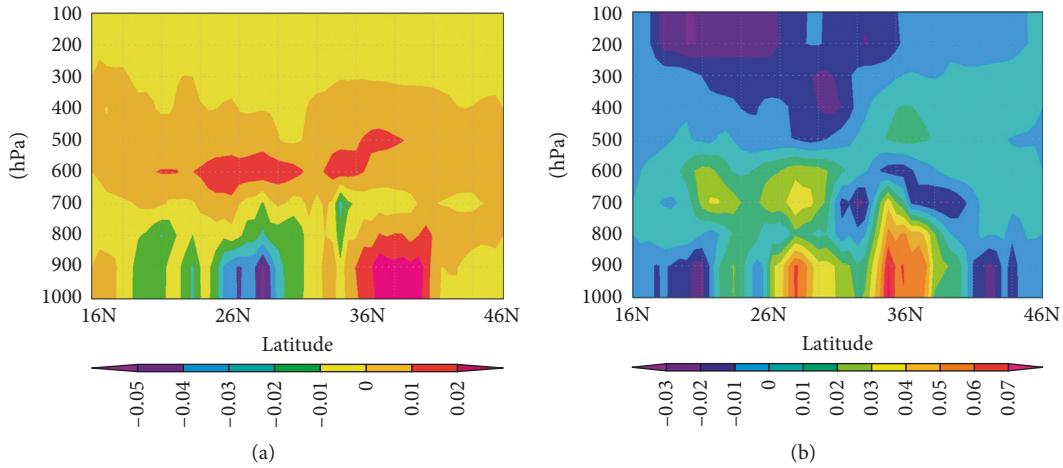

Figure 10: Zonal average temperature changes (K) due to BC aerosols. (a) Summer. (b) Winter.

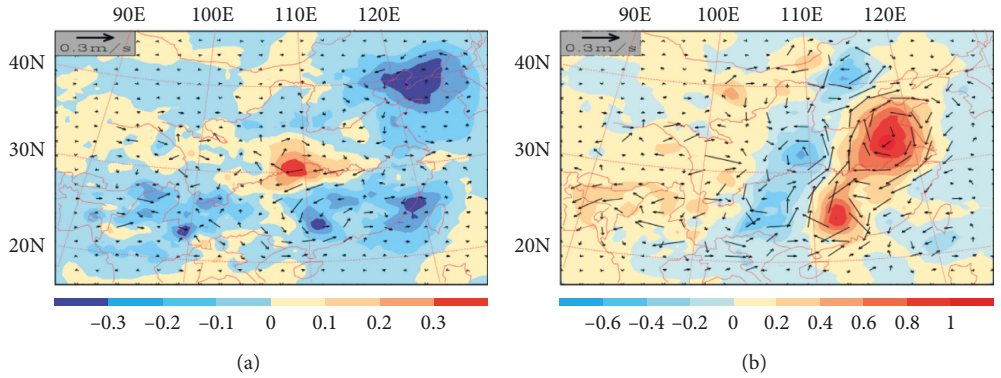

Figure 11: Changes of the average height field and wind field (m/s) at 850 hPa. (a) Summer. (b) Winter.

in most regions of central and southern China. The change of the ground surface temperature caused by BC aerosols is different in the winter than in the summer, and the temperatures increase in most regions of central and eastern China. In the region between the Yangtze River and the Yellow River Basin, the increases in ground surface temperature are significant, and the maximum warming is 0.42 K. In the Yangtze River Delta area, the ground surface temperatures decrease. The temperature decrease in winter can also be seen in Figure 10. In general, the changes of ground surface temperature corresponds relatively well to the changes of sea surface pressure in the winter (an increase in the ground surface temperature corresponds to a decrease in the sea surface pressure), which is coincident with other studies [37]. In the summer, the BC aerosols increase the temperature in some coastal regions in eastern China and intensify the difference in the thermodynamic properties of both the sea and mainland. In the winter, however, warming occurs in some coastal regions in eastern China, and the difference in the thermodynamic properties of the sea and mainland decreases. In general, the change in temperature at the 500 hPa height is smaller than that at the ground surface.

Figure 10 shows the vertical distribution of the zonal average temperature changes caused by BC aerosols during the summer and winter. During the summer, in the region from 21°N to 31°N, the BC aerosols cause cooling of the boundary layer, and the maximum temperature decrease is −0.05 K. Also as seen in Figure 12(a), the surface temperature decreases due to BC in summer. In the region from 33°N to 41°N, the warming caused by the BC aerosols reaches approximately the 300 hPa height, and the maximum warming is 0.02 K. At heights from 700 hPa to 300 hPa, the BC aerosols generally cause the temperatures to increase. At heights above 200 hPa, the BC aerosols cause weak cooling. In the winter, BC aerosols cause temperature increases in most regions at heights below 500 hPa, and the temperature changes in the middle and high atmosphere are relatively weak. This is coincident with the temperature changes shown in Figure 12. Warming centers are located near 26°N and 36°N, and the maximum warming exceeds 0.07 K.

Figure 13 shows the influence of BC aerosols on the precipitation in China during the summer and winter. Not the same as the temperature changes, the precipitation changes caused by BC show more uncertainty which make the distribution more complicated [21]. During the summer, the BC aerosols cause increases of precipitation in southern China and some regions north of the Yellow River. On the other hand, in the Yangtze River Basin and some regions of

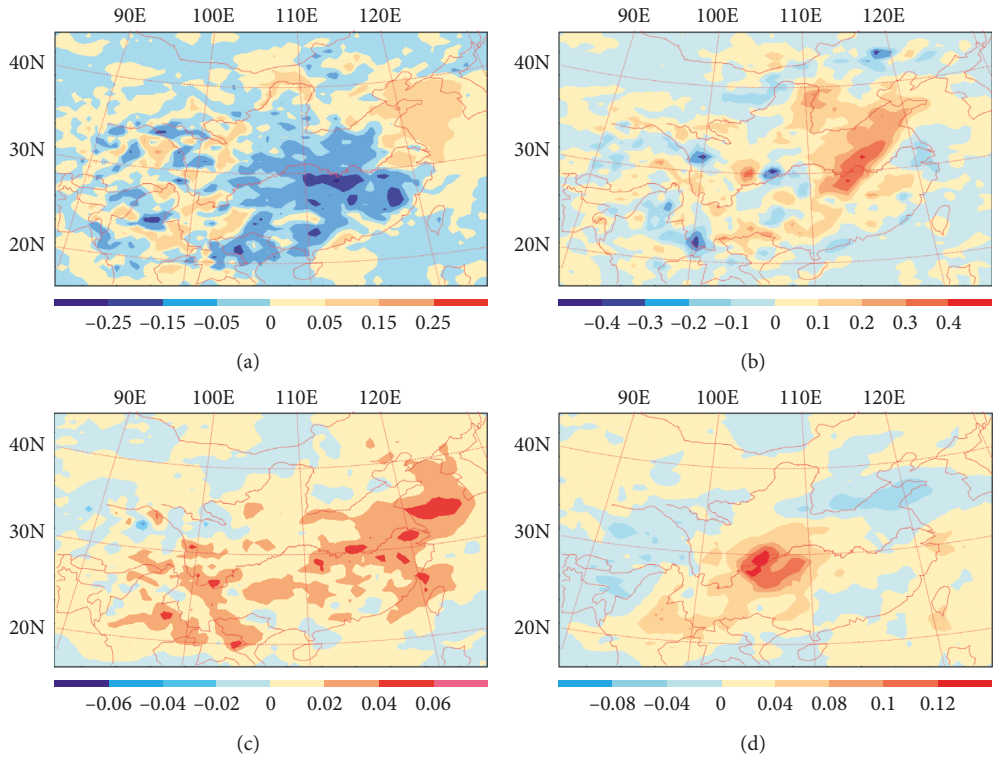

Figure 12: Changes of ground surface temperature (K) caused by BC aerosols. (a) Ground surface in the summer. (b) Ground surface in the winter. (c) 500 hPa height in the summer. (d) 500 hPa height in the winter.

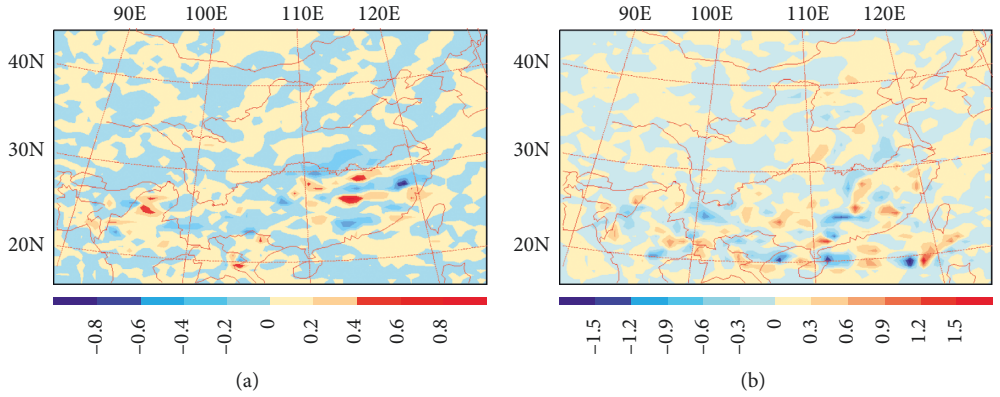

Figure 13: Distributions of the changes of precipitation (mm/d) caused by BC aerosols in China. (a) Summer. (b) Winter.

Northeast China, the precipitation decreases, which is similar to the simulation results of Zhuang et al. [37]. In the winter, the BC aerosols cause increases in precipitation in most areas of central and eastern China; however, in some regions near the Yangtze River Basin, the precipitation decreases.

4.2.6. Average Direct Radiation and the Climate Effect of Black Carbon in Different Regions of China. The climate effect of BC aerosols has significant regional uncertainty. Based on the regional division shown in Chapter 4, Table 1 lists the average direct radiative forcing and climate effects of BC aerosols in five typical regions. The statistical data indicate that the BC aerosols are relatively concentrated in East China and North China, and the all-sky TRF values of BC aerosols are high in East China and North China with regional averages of 1.36 and 1.06 W/m^2, respectively. The regional average clear-sky TRF values of BC aerosols are the same in East China and North China (0.94 W/m^2). The BC aerosols directly cause increases in the ground surface temperatures in East China, North China, and central China, and the average increases are 0.037 K, 0.034 K, and 0.02 K, respectively. In South China, however, the BC aerosols have a cooling effect, and the average temperature decrease is −0.017 K. At the regional scale, BC aerosols increase the ground surface temperatures over the entire domain region. The factors that control the precipitation are very

complicated, such as circulation, radiation, and water vapor. Therefore, the distribution of the influence of BC aerosols on the precipitation is random and irregular. At the regional scale, BC aerosols decrease the precipitation in South China, Northeast China, North China, and East China by 0.11, 0.13, 0.05, and 0.83 mm/d, respectively. In central China, BC aerosols increase the precipitation by 0.01 mm/d. Over the entire domain, the regional average reduction of precipitation caused by BC aerosols is 0.02 mm/d.

5. Summary

In numerical simulations, the optical parameters of aerosols can directly affect the radiation properties. The optical parameters of BC aerosols are related to the particle size and the complex refractive index. Therefore, based on the size-resolved scheme used in previous studies, we use the principle of Mie scattering to calculate the optical parameters of BC aerosols of different scales and apply the new optical parameters to simulate the concentration distribution, radiative forcing, and climate effects of BC aerosols. We also compare the results with simulation results that use the conventional scheme and analyze the effects of the optical parameters on the simulation of the climate effects of BC aerosols.

In comparison with the conventional homogeneous parameterization scheme, the concentrations of the first mode of BC aerosols simulated with the optical parameters recalculated according to the particle size were higher, and the maximum increase was 3.30 $\mu g/m^3$. The concentrations of the other modes of BC aerosols were lower, the total BC aerosol concentration was also lower, and the range of the reductions was −0.2 to −2.8 $\mu g/m^3$. The regional average changes of the BC aerosol column concentrations for the different modes were 0.085, −0.095, −0.089, and −0.054 mg/m^2. The BC aerosol optical thicknesses varied by −0.008 to −0.0064.

In general, the changes in the clear-sky direct radiative forcing of BC aerosols are similar to the distribution of the change in its optical thickness and concentration changes. The regional average clear-sky radiative forcing of BC aerosols decreases by 0.034 W/m^2. The distributions of the influence of BC aerosols on the ground surface temperatures simulated with the two optical parameterization schemes are similar in many regions, but the warming region and the magnitude of warming simulated with the new scheme are smaller. However, the simulated cooling effect is enhanced in some regions, and the variation of the cooling is from −0.04 to −0.24 K.

The simulation of BC aerosols using Scheme 2 enhances the precipitation in South China even more, and the variation is from 0.4 to 2.4 mm/d. In some regions in the middle and lower reaches of the Yangtze River Basin, the BC aerosols cause greater reductions in precipitation (−0.4 to −2.4 mm/d). The influence of BC aerosols on precipitation is complicated and variable, and the difference in the optical parameterization scheme also causes various factors to influence the precipitation, which merits further study.

Comparisons with observations show that Scheme 2 can relatively accurately simulate the ground surface concentrations of BC aerosols. The simulation results indicate that the regional average ground surface concentrations for BC aerosols with the four particle sizes are 0.372, 0.264, 0.055, and 0.004 $\mu g/m^3$. The proportions of the first and second modes, which have relatively small radii, are 53% and 38%, respectively, and the proportions of the third and fourth modes are very small. The regional average total ground surface BC aerosol concentration is 0.69 $\mu g/m^3$. The distribution of the column concentrations is similar to that of the ground surface concentrations. The regional average total BC aerosol column concentration is 0.28 mg/m^2, and the maximum is 2.06 mg/m^2. Regions of high BC aerosol concentrations are located in the Sichuan Basin and the North China Plain and are related to the spatial distribution of their emissions and wind fields. The concentrations of BC aerosols in the spring and summer are higher than those in the other seasons. The regional average BC aerosol optical thickness is 0.0013, and the maximum is 0.0073. The maximum direct radiative forcing of BC aerosols under all-sky conditions is 2.11 W/m^2. The region of high values of the clear-sky radiative forcing is located to the north of the Yellow River, and the maximum value is 1.98 W/m^2. The regional average clear-sky and all-sky TRF values of BC aerosols are 0.49 and 0.36 W/m^2, respectively.

In most regions of East China, North China, and central China, BC aerosols cause increases in the annual average ground surface temperature, which ranges from 0.05 to 0.15 K. In South China and some regions of Northwest China, BC aerosols cause decreases in temperature, and the cooling ranges from 0.05 to 0.15 K. At the regional scale, BC aerosols cause decreases in the annual average precipitation in East China, North China, South China, and Northeast China of −0.83, −0.05, −0.11, and −0.13 mm/d, respectively. In central China, BC aerosols cause the annual average precipitation to increase by 0.01 mm/d. In the winter and summer, the region where the 850 hPa height field decreases corresponds to a convergence of the wind field. The change in airflow caused by BC aerosols in the winter is greater than that in the summer. In the winter, BC aerosols cause a greater increase in the ground surface temperature. In the region between the Yangtze River and the Yellow River Basin, the increase in the ground surface temperature is significant, and the maximum warming is 0.42 K. During the summer, BC aerosols increase the precipitation in southern China and some regions to the north of the Yellow River. However, in the Yangtze River Basin and some regions of Northeast China, BC aerosols decrease the precipitation. There are good correlations between the changes of circulation, pressure, and temperature induced by BC aerosols.

The climate effects of BC are related to its size distributions, and when using other size distributions, the results will change. This may be discussed in more detail in later studies. The results of this paper are related to the mixing sate of BC, and we just considered the simple situation. Taking the mixing state of BC and other aerosols into consideration may show different results.

Data Availability

The data used to support the findings of this study are available from the corresponding author upon request.

Conflicts of Interest

The authors declare that they have no conflicts of interest.

Acknowledgments

This study was supported by the National Key Basic Research and Development Planning Program of China (Program 973) (2014CB441203), National Key Research and Development Program of China (2017YFC0209600), and National Natural Science Foundation of China (41575141). The numerical calculations in this paper have been done on the Blade cluster system in the High Performance Computing and Massive Data Center (HPC&MDC) of School of Atmospheric Science, Nanjing University. We thank the High-Performance Computing Center at Nanjing University. We acknowledge the BC emission inventory in the MEIC (Multi-resolution Emission Inventory for China) data provided by Professor Q. Zhang from Tsinghua University, China (http://www.meicmodel.org).

References

[1] V. Ramanathan and G. Carmichael, "Global and regional climate changes due to black carbon," *Nature Geoscience*, vol. 1, no. 1, pp. 221–227, 2008.

[2] T. Bond, S. Doherty, D. Fahey et al., "Bounding the role of black carbon in the climate system: a scientific assessment," *Journal of Geophysical Research: Atmospheres*, vol. 118, no. 11, pp. 5380–5552, 2013.

[3] IPCC, *Climate Change 2013: The Physical Science Basis. Contribution of Working Group I to the Fifth Assessment Report of the Intergovernmental Panel on Climate Change*, Cambridge University Press, Cambridge, UK, 2013.

[4] R. C. Levy, L. A. Remer, and O. Dubovik, "Global aerosol optical properties and application to moderate resolution imaging spectroradiometer aerosol retrieval over land," *Journal of Geophysical Research*, vol. 112, no. 112, pp. 3710-3711, 2007.

[5] F. S. Wei, "Some thinking on the formulation of SO_2 emission and its quality in China," *Chinese Journal of Environmental Monitoring*, vol. 11, no. 4, p. 22, 1995, in Chinese.

[6] J. R. Sun and Y. Liu, "Possible effects of aerosols from China on East Asia summer monsoon: the complex effects of black carbon aerosols and sulfate aerosols," *Journal of Climate Change Research*, vol. 4, no. 3, pp. 161–166, 2008.

[7] S. Menon, J. Hansen, L. Nazarenko, and Y. Luo, "Climate effects of black carbon aerosols in China and India," *Science*, vol. 297, no. 5590, pp. 2250–2253, 2002.

[8] M. Z. Jacobson, "Control of fossil-fuel particulate black carbon and organic matter, possibly the most effective method of slowing global warming," *Journal of Geophysical Research*, vol. 107, no. D19, p. 4410, 2002.

[9] J. E. Penner, H. Eddleman, and T. Novakov, "Towards the development of a global inventory for black carbon emissions," *Atmospheric Environment. Part A. General Topics*, vol. 27, no. 8, pp. 1277–1295, 1993.

[10] W. F. Cooke, C. Liousse, H. Cachier et al., "Construction of a 1×1 fossil fuel emission data set for carbonaceous aerosol and implementation and radiative impact in the ECHAM4 model," *Journal of Geophysical Research: Atmospheres*, vol. 104, no. D18, pp. 22137–22162, 1999.

[11] D. G. Streets, S. Gupta, S. T. Waldhoff, M. Q. Wang, T. C. Bond, and Y. Y. Bo, "Black carbon emissions in China," *Atmospheric Environment*, vol. 35, no. 25, pp. 4281–4296, 2001.

[12] J. M. Ge, Y. Z. Liu, and J. P. Huang, "Optical characteristics of black carbon and dust aerosols with HITRAN data," *Journal of Applied Optics*, vol. 30, no. 2, pp. 202–209, 2009.

[13] S. E. Bauer, S. Menon, D. Koch, T. C. Bond, and K. Tsigaridis, "A global modeling study on carbonaceous aerosol microphysical characteristics and radiative effects," *Atmospheric Chemistry and Physics*, vol. 10, no. 15, pp. 7439–7456, 2010.

[14] D. V. Spracklen, K. S. Carslaw, U. Pöschl, A. Rap, and P. M. Forster, "Global cloud condensation nuclei influenced by carbonaceous combustion aerosol," *Atmospheric Chemistry and Physics*, vol. 11, pp. 9067–9087, 2011.

[15] X. Ma, H. Liu, J. J. Liu et al., "Sensitivity of climate effects of black carbon in China to its size distributions," *Atmospheric Research*, vol. 185, pp. 118–130, 2016.

[16] E. P. Shettie and R. W. Fenn, *Models for the Aerosols of the Lower Annosphere and the Effect of Humidity Variations on their Optical Properties*, Air Force Geophysical Laboratory, AFGL-TR-79~0214, Bedford, MA, USA, 1979.

[17] J. H. Ma, Y. F. Zheng, and H. Zhang, "The optical depth global distribution of black carbon aerosol and its possible reason analysis," *Journal of the Meteorological Sciences*, vol. 12, no. 2, pp. 156–164, 2007, in Chinese.

[18] J. W. Winchester, W. X. Lu, L. X. Ren et al., "Fine and coarse aerosol composition from a rural area in northern China," *Atmospheric Environment*, vol. 15, no. 6, pp. 933–937, 1981.

[19] L. L. Li, J. Su, Q. Fu et al., "Parameterization of radiation properties of dust aerosols," *Atmospheric Physics and Atmospheric Environment*, vol. S18, 2012.

[20] K. N. Liou and R. Davies, "Radiation and cloud processes in the atmosphere," *Physics Today*, vol. 46, no. 46, pp. 66-67, 1993.

[21] J. J. Shang, H. Liao, Y. Fu et al., "The impact of sulfate and black carbon aerosols on summertime cloud properties in China," *Journal of Tropical Meteorology*, vol. 4, no. 16, pp. 451–466, 2017.

[22] P. B. Guan, H. D. Shi, Q. X. Gao et al., "Study on black carbon aerosol simulation of climate effect in China," *Journal of Environmental Engineering Technology*, vol. 7, no. 4, pp. 418–423, 2017, in Chinese.

[23] L. R. Chen, H. H. Zheng, H. D. Shi et al., "Simulation of impact of future black carbon aerosol emission on regional climate change," *Journal of Environmental Engineering Technology*, vol. 8, no. 1, pp. 1–11, 2018, in Chinese.

[24] T. M. Fu, J. J. Cao, X. Y. Zhang et al., "Carbonaceous aerosols in China: top-down constraints on primary sources and estimation of secondary contribution," *Atmospheric Chemistry and Physics*, vol. 12, no. 5, pp. 2725–2746, 2012.

[25] K. Li, H. Liao, Y. H. Ma, and A. R. David, "Source sector and region contributions to concentration and direct radiative forcing of black carbon in China," *Atmospheric Environment*, vol. 124, pp. 351–356, 2015.

[26] H. N. Liu, W. M. Jiang, J. P. Tang, and X. Li, "A numerical study on the troposphere photochemical oxidation process of sulfur dioxide over China," *Chinese Journal of Environmental Sciences*, vol. 21, no. 3, pp. 359–363, 2001.

[27] H. N. Liu, L. Zhang, and J. Wu, "A modeling study of the climate effects of sulfate and carbonaceous aerosols over China," *Advances in Atmospheric Sciences*, vol. 27, no. 6, pp. 1276–1288, 2010.

[28] L. Zhang, H. N. Liu, and N. Zhang, "Impacts of internally and externally mixed anthropogenic sulfate and carbonaceous aerosols on east Asian climate," *Acta Meteorol Sinica*, vol. 5, no. 5, pp. 639–658, 2011.

[29] H. Z. Chen, D. Wu, B. T. Liao, H. Y. Li, and F. Li, "Compare of black carbon concentration variation between Dongguan and Maofengshan," *China Environmental Science*, vol. 33, no. 4, pp. 605–612, 2013.

[30] Y. J. Li, L. Zhang, X. J. Cao, Y. Yue, and J. S. Shi, "Property of black carbon concentration over urban and suburban of Lanzhou," *China Environmental Science*, vol. 34, no. 6, pp. 1397–1403, 2014, in Chinese.

[31] H. N. Liu, Y. Zhu, H. J. Lin, and X. Y. Wang, "Observation and analysis of haze characteristics in Suzhou based on automatic station data," *China Environmental Science*, vol. 35, no. 3, pp. 668–675, 2015, in Chinese.

[32] G. L. Qiu, N. Liu, and X. B. Feng, "Pollution characteristics of atmospheric black carbon in Guiyang, Guizhouprovince, Southwest China," *Chinese Journal of Ecology*, vol. 30, no. 5, pp. 1018–1022, 2011, in Chinese.

[33] X. L. Sun and Y. F. Suo, "The observation study of black carbon concentration in Guilin during 2012," *Journal of Meteorological Research and Application*, vol. 34, pp. 130-131, 2013, in Chinese.

[34] Y. F. Wang, Y. J. Ma, Z. Y. Lu, D. P. Zhou, N. W. Liu, and Y. H. Zhang, "In situ continuous observation of atmospheric black carbon aerosol mass concentration in Liaoning region," *Research of Environmental Sciences*, vol. 24, no. 10, pp. 1088–1096, 2011, in Chinese.

[35] X. Zhang, J. Tang, Y. F. Wu, J. Wu, P. Yan, and R. J. Zhang, "Variations of black carbon aerosol observed in Beijing and surrounding area during 2006-2012," *China Powder Science and Technology*, vol. 21, no. 4, pp. 24–29, 2015, in Chinese.

[36] P. S. Zhao, F. Dong, Y. D. Yang et al., "Characteristics of carbonaceous aerosol in the region of Beijing, Tianjin, and Hebei, China," *Atmospheric Environment*, vol. 71, no. 3, pp. 389–398, 2013.

[37] B. L. Zhuang, F. Jiang, T. J. Wang, S. Li, and B. Zhu, "Investigation on the direct radiative effect of fossil fuel black-carbon aerosol over China," *Theoretical and Applied Climatology*, vol. 104, pp. 301–312, 2010.

[38] Y. Qian, L. R. Leung, S. J. Ghan, and F. Giorgi, "Regional climate effects of aerosols over China: modeling and observation," *Tellus B*, vol. 55, pp. 914–934, 2003.

[39] H. Zhang, Z. L. Wang, P. W. Guo, and Z. Z. Wang, "A modeling study of the effects of direct radiative forcing due to carbonaceous aerosol on the climate in east Asia," *Advances in Atmospheric Sciences*, vol. 26, no. 1, pp. 57–66, 2009.

[40] L. Liao, S. Lou, Y. Fu et al., "Radiative forcing of aerosols and its impact on surface air temperature on the synoptic scale in eastern China," *Chinese Journal of Atmospheric Sciences*, vol. 39, no. 1, pp. 68–82, 2015, in Chinese.

[41] H. Liao and J. H. Seinfeld, "Effect of clouds on direct aerosol radiative forcing of climate," *Journal of Aerosol Science*, vol. 28, no. D4, pp. 3781–3788, 1997.

[42] L. S. Chang and S. U. Park, "Direct radiative forcing due to anthropogenic aerosols in east Asia during April 2001," *Atmospheric Environment*, vol. 38, no. 27, pp. 4467–4482, 2004, in Chinese.

[43] J. Wu, W. M. Jiang, H. N. Liu, W. G. Wang, and Y. Luo, "Comparison of on-line and off-line simulation methods for direct radiative forcing of anthropogenic sulfate," *Acta Meteorologica Sinica*, vol. 62, no. 4, pp. 486–492, 2004, in Chinese.

[44] W. Y. Chang and H. Liao, "Anthropogenic direct radiative forcing of tropospheric ozone and aerosols from 1850 to 2000 estimated with IPCC AR5 emissions inventories," *Atmospheric and Oceanic Science Letters*, vol. 2, article 201e207, 2009.

[45] P. P. Wu and Z. W. Han, "Indirect Radiative and Climatic Effects of Sulfate and Organic Carbon Aerosols over East Asia Investigated by RIEMS," *Atmospheric and Oceanic Science Letters*, vol. 4, no. 1, pp. 7–11, 2011.

[46] L. Guo, E. J. Highwood, L. C. Shaffrey, and A. G. Turner, "The effect of regional changes in anthropogenic aerosols on rainfall of the east Asian summer monsoon," *Atmospheric Chemistry and Physics Discuss*, vol. 12, no. 9, pp. 23007–23038, 2012, in Chinese.

[47] Y. Q. Jiang, X. Q. Yang, and X. H. Liu, "Seasonality in anthropogenic aerosol effects on east Asian climate simulated with CAM5," *Journal of Geophysical Research*, vol. 120, no. 20, pp. 10837–10861, 2015.

[48] B. L. Zhuang, S. Li, T. J. Wang et al., "Direct radiative forcing and climate effects of anthropogenic aerosols with different mixing state over China," *Atmospheric Environment*, vol. 79, pp. 349–361, 2013.

[49] D. D. Wang, B. Zhu, Z. H. Jiang et al., "A modeling study of effects of anthropogenic aerosol on east Asian winter monsoon over eastern China," *Transactions of Atmospheric Sciences*, vol. 40, no. 4, pp. 541–552, 2017, in Chinese.

[50] A. S. Ackerman, O. B. Toon, D. E. Stevens et al., "Reduction of tropical cloudiness by soot," *Science*, vol. 288, no. 5468, pp. 1042–1047, 2000.

[51] J. E. Kristjánsson, "Studies of the aerosol indirect effect from sulfate and black carbon aerosols," *Journal of Geophysical Research*, vol. 107, no. D15, 2002.

[52] E. J. Highwood and R. P. Kinnersley, "When smoke gets in our eyes: the multiple impacts of atmospheric black carbon on climate, air quality and health," *Environment International*, vol. 32, no. 4, pp. 560–566, 2006.